RESEARCH/REVIEW ARTICLE

Impact of summertime anthropogenic emissions on atmospheric black carbon at Ny-Ålesund in the Arctic

Jianqiong Zhan & Yuan Gao

Department of Earth & Environmental Sciences, Rutgers University, 101 Warren Street, Newark NJ 07102, USA

Abstract

Measurements of equivalent black carbon (EBC), calculated from aethalometer measurements of light attenuation, were carried out in July 2011 at Ny-Ålesund in the Arctic. Highly elevated EBC concentrations were observed within the settlement of Ny-Ålesund, with a median value of 17 ng m^{-3}, which was about two times the background level. Results from the ensemble empirical mode decomposition method suggested that about 60–80% of atmospheric EBC concentrations at Ny-Ålesund were from local emissions, while only 20–40% arrived via atmospheric transport. The estimated average local emission rate was 8.1 g h^{-1}, with an uncertainty of approximately a factor of two. The pollution plume was confined to 10 km downwind of the settlement, with the total EBC deposition estimated to be 6.4–44 ng m^{-2} h^{-1}. This may affect snow black carbon (BC) concentrations in nearby glaciated areas. The efficiencies of the long-range transport were estimated based on cluster analysis and potential precipitation contribution function, and the results implied that transport from western Europe is more efficient than from central Russia, on account of relatively rapid transport from western Europe and infrequent precipitation along this route. However, there was no correlation between air mass back-trajectories and EBC concentrations, suggesting that the contribution of long-range transport to EBC measured in Ny-Ålesund might be not significant in this season.

Black carbon (BC) in the atmosphere affects the radiative balance of the Arctic due to its strong light absorption (Shindell & Faluvegi 2009). Although organic carbon has an overall cooling effect on the atmosphere (Solomon et al. 2007), for the highly reflective snow/ice surface of the Arctic, the mixtures of organic carbon and BC still exert positive top-of-atmosphere radiative forcing (Flanner et al. 2009). The impact of BC can continue even after it is removed from the atmosphere and deposited on ice or snow, through the reduction of surface albedo (Doherty et al. 2010; Hadley & Kirchstetter 2012). Over the 20th century, about 20% of the warming and snow/ice-cover melting in the Arctic is due to the BC-albedo effect (Koch et al. 2011). These findings identify BC as a critical climate forcing agent in the Arctic.

Several ground- and aircraft-based investigations of atmospheric BC have been carried out in the Arctic. Annual mean concentrations of BC ranged from 26 to 49 ng m^{-3}, with values at Alert and Zeppelin Station higher than those at Barrow and Summit (Hirdman, Sodemann et al. 2010). A pronounced seasonal cycle has been found, with a maximum in winter/early spring (i.e., the haze season) and a minimum in summer (Sharma et al. 2006; Eleftheriadis et al. 2009). Strong seasonal variations are consistent with atmospheric transport patterns in the Arctic (Stohl 2006; Hirdman, Burkhart et al. 2010). Vertical concentration profiles of BC were observed during the Arctic Research of the Composition of the Troposphere from Aircraft and Satellites mission in 2008. In the spring, two peaks were revealed in the profile of BC mass mixing

1

ratio: one was at 5.5 km, with a mass mixing ratio of 150 ng kg^{-1} in the aged air mass; the other one, at 4.5 km, had a mass mixing ratio of 250 ng kg^{-1} and was associated with biomass burning (Spackman et al. 2010). The vertical stratification of BC increased with altitude at lower altitudes (650 hPa), whereas at higher altitudes it decreased toward the middle troposphere (Jacob et al. 2010; Spackman et al. 2010). The summertime BC concentrations varied between 5 and 100 ng kg^{-1} from 0 to 12 km in altitude, with higher BC concentrations in the lower troposphere in July. As there were widespread fires during the aircraft campaigns, the enhancement of BC could have resulted from increased biomass burning (Spackman et al. 2010), which might not be representative of typical BC distributions in summer. Northern Eurasia has repeatedly been shown to be the major source for the BC concentrations observed at the Arctic surface stations in winter and spring (Stohl 2006; Hirdman, Burkhart et al. 2010). In summer, transport from the surrounding continental locations is limited by the weaker and more northern extent of the polar dome (Klonecki et al. 2003; Law & Stohl 2007) as well as more frequent precipitation (Barrie 1996; Bourgeois & Bey 2011). As result of low efficiency of long-range transport, local aerosol sources become much more important in summer.

Recent studies have highlighted the role of local emissions within the Arctic. Measurements made at Barrow, Alert and Zeppelin Station over more than a decade have indicated that BC concentrations measured in the Arctic are highly sensitive to emissions within the Arctic (Hirdman, Sodemann et al. 2010). In the last 10 years, human activities such as general transport (aviation and shipping), oil and gas flaring and resource exploitation have increased; these could lead to strongly elevated concentrations of BC in the Arctic (Granier et al. 2006; Dalsøren et al. 2007; Lack et al. 2008; Vestreng et al. 2009; Corbett et al. 2010; Lee et al. 2010; DeAngelo 2011; Quinn et al. 2011). Around 4.5 Gg yr^{-1} of BC is contributed from Arctic shipping, and this may increase global climate forcing by at least 17% compared to warming due to CO_2 emissions from these vessels (ca. 42 000 Gg yr^{-1}; Corbett et al. 2010). Lee et al. (2010) also highlighted aviation emissions associated with major routes in the vicinity of 60°N. Johnson et al. (2011) suggested the mean soot emission rate is 2.0 g s^{-1} at a calculated uncertainty of 33%, from measurement of the emission rate from oil and gas flaring in Uzbekistan. However, these emissions are still not well characterized and specific emission factors are still uncertain due to the lack of measurements at many locations. In Svalbard, local human activities, such as motor vehicle use, electric power production and domestic combustion, persistently occur, contributing to

the loading of BC in the air, but more quantitative evaluations of these contributions are needed.

To characterize the anthropogenic emissions affecting the BC concentration in Svalbard, field measurements were carried out within and near the settlement of Ny-Ålesund in July 2011, the peak season of local human activities. In this paper, we present the measurement results and estimate the contribution of local emissions, the emission rates and the BC deposition rates using model simulations. These results will be useful for interpreting other data sets in the region, for planning future measurement campaigns in this region and for developing emission reduction strategies in the Arctic.

Methods

Measurement sites

The measurements were made in Ny-Ålesund, on the island of Spitsbergen in the Svalbard Archipelago. The sampling sites were one site at the Chinese Yellow River Station (YRS) (78.92°N, 11.93°E, 13 m a.s.l) within the Ny-Ålesund settlement and three sites around Ny-Ålesund: S2 (78.90°N, 12.07°E, 126 m a.s.l), S3 (78.99°N, 12.06°E, 134 m a.s.l) and S4 (78.96°N 11.60°E, 33 m a.s.l; Fig. 1). Data measured at Zeppelin Station (78.90°N, 11.88°E, 474 m a.s.l) by Eleftheriadis et al. (2009) were used in this study for comparison. Zeppelin Station is situated on the mountain of Zeppelinfjellet, 1 km south of, and over 400 m above, the settlement, where contaminants from Ny-Ålesund are minimal (Hirdman, Sodemann et al. 2010). The YRS is situated in Ny-Ålesund, directly below Zeppelin Station; it was therefore directly affected by local emissions from tourism and research-related activities in the settlement. S2 was located 4 km south-east of Ny-Ålesund, on the glacier Midtre Lovénbreen. S3 lay on the island of Blomstrandhalvøya, on the other side of the fjord from Ny-Ålesund and at a distance of about 5 km from the settlement. S4 was situated on the coastal plain of Kvadehuksletta at the north-west point of the peninsula Brøggerhalvøya, about 10 km away from Ny-Ålesund.

BC measurement and meteorological data collection

Aethalometers have been widely used for measuring BC concentrations in the Arctic (Sharma et al. 2006; Eleftheriadis et al. 2009; Hirdman, Burkhart et al. 2010). The device measures the attenuation of light transmitted through particles that accumulate on a quartz fibre filter and interprets the rate of increase of optical attenuation
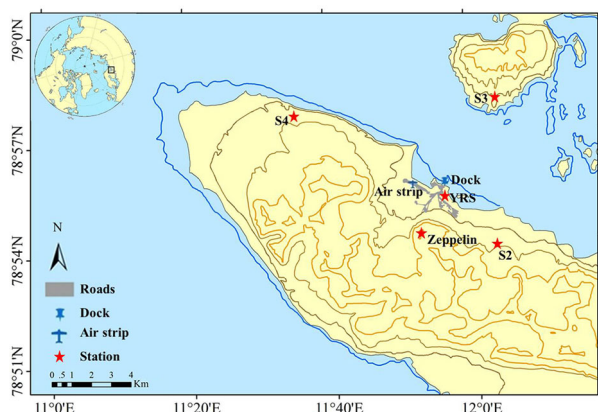
Fig. 1 Map of the peninsula Brøggerhalvøya, showing the locations of Ny-Ålesund and the sampling sites: Chinese Yellow River Station (YRS, 11.93°E, 78.92°N, 13 m a.s.l), S2 (12.07°E, 78.90°N, 126 m a.s.l), S3 (12.06°E, 78.99°N, 134 m a.s.l), S4 (11.60°E, 78.96°N, 33 m a.s.l).

in terms of the concentration of optically absorbing material in the sample air stream. Since these optically based measurements rely on some assumptions to convert particle light absorption to BC concentrations, the data derived from this method are also called equivalent BC (EBC; Sharma et al. 2004). In this study, an AE42 Model Aethalometer (7-wavelength; only λ ca. 880 nm reported here; Magee Scientific, Berkeley, CA, USA) was used at the YRS site, while model AE51 instruments (Magee Scientific) were used at sites S2, S3 and S4. Temporal resolutions were 10 min for the AE42 unit and 5 min for the AE51 units during the measuring period of 5–19 July 2011. The specific mass absorption coefficient $\alpha_{ap} = 15.9$ m^2 g^{-1} was used to calculate BC mass concentrations from the AE42 device. This value was derived from simultaneous measurements of light absorption and thermo-optical elemental carbon mass concentration by Nyeki et al. (2005), which was also applied in EBC calculations at Zeppelin Station by Eleftheriadis et al. (2009). Data from the AE51 units were corrected by comparing AE42 and AE51 measurements at the same place.

The scattering correction wasn't employed in this study since aerosols in these remote areas were well-aged, requiring little or no correction (Hansen et al. 2007).The overall uncertainty on the aggregated data is on the order of 10% (Hansen et al. 2007). To circumvent the potential error induced through the use of two different instruments, co-location experiments were carried out both before and after experiments. Measurement data are summarized in Table 1.

Meteorological parameters, for example, air temperature, wind speed, wind and relative humidity, were collected simultaneously with a temporal resolution of one hour. Precipitation data were from Ny-Ålesund station, which is around 0.2 km away from YRS. The arithmetic mean, maximum and minimum for each parameter are presented in Table 2.

Atmospheric transport and dispersion model

The Hybrid Single-Particle Lagrangian Integrated Trajectory 4 (HYSPLIT_4) model, created by the US National Ocean and Atmospheric Administration (Draxler & Hess 1998), was used to generate both forward and backward trajectories and complex dispersion/deposition simulations, using US National Centers for Environmental Prediction/National Center for Atmospheric Research (NCAR/NCEP) reanalysis data. The data were provided at a horizontal resolution of 2.5° × 2.5°, 17 vertical levels up to 10 hPa, and a temporal resolution of six hours. Emission rates were estimated by fitting the predications from dispersion model to the observed concentration difference between within and outside the community, and then the subsequent advection, dispersion and deposition of EBC were simulated, using NCAR/NCEP reanalysis meteorological data fed into the HYSPLIT model. Wet deposition was calculated using precipitation data from the European Centre for Medium-Range Weather Forecasts (ECMWF). The washout ratio was calculated from the Scott washout ratio (Scott 1978).

Table 1 Comparison of equivalent black carbon (EBC) concentrations in Svalbard, Alert (Nunavut) and Barrow (Alaska).

Station	Location	EBC concentration (ng m^{-3})[a]	Time period	References
Yellow River Station	11.93°E, 78.92°N, 13 m a.s.l	17 (4.1–38)	July 2011	This work
S2	12.07°E, 78.90°N, 126 m a.s.l	5.3 (1.0–7.8)	July 2011	This work
S3	12.06°E, 78.99°N, 134 m a.s.l	6.6 (0.0–15)	July 2011	This work
S4	11.60°E, 78.96°N, 33 m a.s.l	4.7 (0.0–12)	July 2011	This work
Zeppelin Station	11.92°E, 78.93°N, 474 m a.s.l	7 (3–11)	Summers 1998–2007	Eleftheriadis et al. 2009
		11	Summers 1990–1992	Heintzenberg & Leck 1994
Gruvebadet	11.92°E, 78.93°N, 10 m a.s.l	5	Summers 1979–1990	Heintzenberg & Leck 1994
Alert	62.3°W, 82.5°N, 210 m a.s.l	12–26	Summers 1989–2003	Sharma et al. 2004, 2006
Barrow	156.6°W, 71.3°N, 11 m a.s.l	9–24	Summers 1989–2003	Sharma et al. 2006

[a]Mean (minimum–maximum).

Table 2 Correlations between equivalent black carbon (EBC) concentration and meteorological parameters at Yellow River Station, Ny-Ålesund. Asterisks indicate correlation significant to the 99% confidence level (two-tailed).

	Mean and range	Correlation coefficient	P
Temperature (°C)	6.5 (2.4–10.5)	0.22*	0.000
Pressure (hPa)	1011.0 (997.2–1023.1)	−0.21*	0.000
Wind speed (m s^{-1})	3.2 (0.0–12.5)	−0.10*	0.000
Total precipitation (mm/day)	0.8 (0.0–11.1)	−0.10*	0.000
Relative humidity (%)	80 (57–93)	0.03	0.125

Time-frequency analysis

To better understand the properties and physical mechanism hidden in the EBC data, ensemble empirical mode decomposition (EEMD) was used to isolate and extract various temporal scales in data. These various temporal scales were further linked to different sources. There are other popular tools, such as Fourier analysis, wavelet analysis and Wigner-Ville distribution, which can also decompose the data into the components of different timescales, but they are limited to either linear or stationary processes, and require a priori function basis. This often makes their applications to data from nonlinear and non-stationary processes problematic. EEMD is an adaptive method that is designed specifically for analysing nonlinear and non-stationary data without imposing irrelevant mathematical rules (Wu & Huang 2009). This approach consists of sifting an ensemble of white noise-added signal, and obtains the mean of corresponding intrinsic mode functions (IMFs) that bear the full physical meaning and a time-frequency distribution, and also gets the corresponding average residual which is identical to the trend. Further details on the EEMD method can be found in Wu & Huang (2009). The results are tested by statistical significance at the 95% confidence level based on a testing method suggested by Wu & Huang (2004) against the white noise null hypothesis.

Results and discussion

EBC concentrations

The concentrations of EBC (Fig. 2) at YRS ranged from 4.1 to 38 ng m^{-3}, with a median value of 17 ng m^{-3}, which was higher than values observed outside the Ny-Ålesund settlement at S2, S3 and S4, where median EBC concentrations were 5.3, 6.6 and 4.4 ng m^{-3}, respectively. The median value found at YRS was in the range of the summer monthly average at Alert (12–26 ng m^{-3}) and Barrow (9–24 ng m^{-3}) from 1989 to 2003 (Sharma et al. 2006), but higher than EBC concentrations at Zeppelin Station (3–11 ng m^{-3}; Eleftheriadis et al. 2009). The levels of EBC at S2, S3 and S4 were comparable to measurements taken at Zeppelin Station (475 m a.s.l) with a median EBC concentration of 7 ng m^{-3} (Eleftheriadis et al. 2009). These levels were also similar to aircraft measurements over the Arctic in July 2008, where the BC mass concentration was ca. 10 ng kg^{-1} above 3 km and ca. 5 ng kg^{-1} below 3 km (Liu et al. 2011) as well as the Gruvebadet sea-level site near YRS (78.92°N, 11.89°E) measured by Heintzenberg & Leck (1994), who reported 5 ng m^{-3} for summer/autumn from 1979 to 1990.

The results showed that the EBC concentration at YRS was higher than the levels of EBC at Zeppelin Station and ground-based stations around the settlement. Similar results were reported by Hermansen et al. (2011): SO$_2$ and soot levels were higher in the Ny-Ålesund settlement than at Zeppelin Station. The aerosol scattering coefficient was also ca. 13–66% lower at Zeppelin, suggesting relative cleanliness at Zeppelin Station due to its elevation at 474 m a.s.l, above a temperature inversion layer, which limited vertical mixing (Di Liberto et al. 2012). Residential emissions were presumably a factor contributing to the elevated EBC concentration at YRS. This observation is further illustrated in Fig. 3. As shown, EBC concentrations corresponded to wind directions; higher EBC concentrations were associated with being downwind—especially south—of Ny-Ålesund. Variations and average EBC concentration during the daytime were larger than those at night, indicating more complicated and stronger sources in the daytime than at night. This confirms that local human activities were one of the major sources affecting the concentration of EBC at Ny-Ålesund.

Local meteorological influences

The relationships between meteorological parameters and EBC concentrations were tested for statistical significance. Pearson's correlation coefficient and principal component regression (PCR) were used to estimate the influence of meteorological parameters on the EBC concentrations. PCR assumes that the variables have normal distributions. However, some of our measured data are not normally distributed; therefore logarithmic
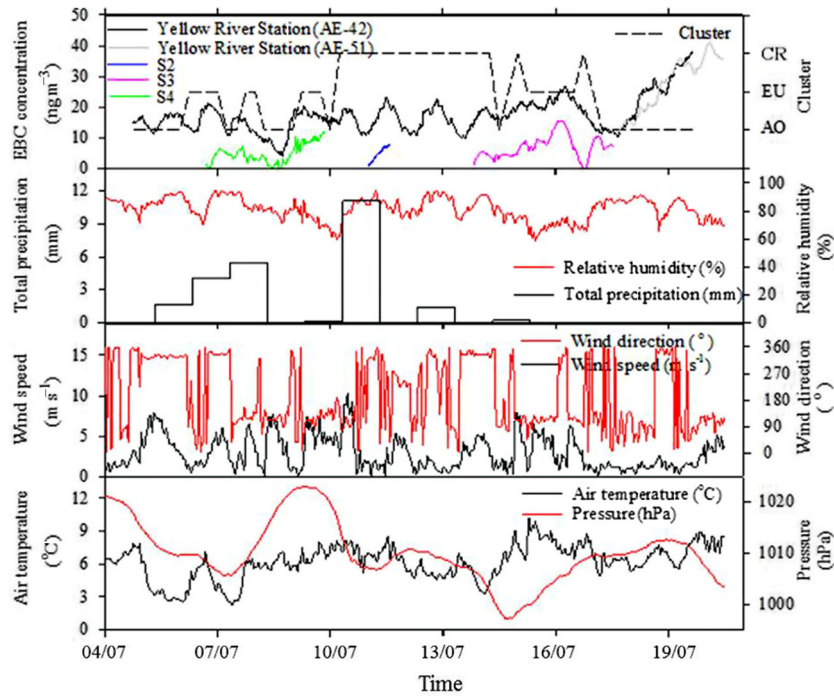
Fig. 2 Time series of equivalent black carbon (EBC) concentrations, air mass transport pathways (dashed line; AO represents the Arctic Ocean sector, EU stands for western Europe and CR stands for central Russia) and meteorological parameters (total precipitation, relative humidity, wind speed, wind direction, air temperature, pressure).

transformations were done for the EBC concentrations, wind speed and relative humidity to avoid violation of the normality assumption.

The levels of EBC were significantly ($P < 0.000$) related to temperature, wind speed, atmospheric pressure and total precipitation (Table 2). Among the meteorological parameters, temperature had the greatest effect on the EBC concentration, with a Pearson's correlation coefficient of 0.22 ($P < 0.000$), indicating higher levels of EBC

Fig. 3 Variations in equivalent black carbon concentration (ng m^{-3}) affected by wind directions at Yellow River Station. Individual wind direction measurements are accumulated and the relative frequency is shown as a percentage.

during higher temperature periods. A negative correlation was found between temperature and boundary layer height, with a Pearson correlation of -0.38 ($P < 0.000$). This suggests that high EBC concentrations in warm air might relate to shallow boundary layer, which was created by temperature inversion (Tjernström 2005). Observations and NCAR/NCEP) reanalysis data reveal that elevated temperature inversion dominates 91% of summer months (Tjernström & Graversen 2009), and this was more pronounced in a warmer summer (e.g., 2007) compared to other years (2003–06 and 2008; Devasthale et al. 2010). Temperature inversion creates a stable and shallow mixing layer, which limits the vertical transfer of EBC between the surface and the free troposphere, trapping EBC close to the ground. This suggests that temperature may indirectly influence EBC concentration when a shallow boundary layer is capped by temperature inversion in the summer.

As expected, a negative correlation was found between EBC concentration and total precipitation due to removal via wet deposition. A negative relationship was found between the EBC concentration and wind speed, with a Pearson correlation of -0.10 ($P < 0.000$), indicating the dilution effect of winds on the EBC concentrations. Relative humidity showed less significant correlation with the EBC concentrations, with a Pearson correlation

of 0.033 ($P = 0.34$), suggesting that humidity did not directly affect EBC concentrations since most of the BC particles were hydrophobic.

The association between selected meteorological parameters (temperature, wind speed, relative humidity, atmospheric pressure and total precipitation) and EBC concentration was analysed by PCR. The selected meteorological parameters can only explain 19% of the variation in EBC concentrations ($P < 0.000$), suggesting that other factors are influencing EBC levels in the area, such as the distance to sources and the strength of sources and sinks.

EBC concentration from local emissions and long-range transport

Ny-Ålesund can be both a source and receptor for pollutants because some are locally generated and some are transported there over long distances. To evaluate these two factors, local emissions were assumed to be generated by both intermittent, short-term activities and continuous activities, while long-range transport, which is controlled by atmospheric circulation, occurs at various temporal scales (Stohl 2006). In order to separate various signals hiding in the data, EEMD was used to decompose the EBC data into various frequency signals. The results included IMFs, which represent some specific scale of oscillation, and a residual that is identical to the trend, expressed as:

$$EBC_{total} = IMF_1 + IMF_2 + \ldots + IMF_n + Trend \quad (1)$$

BC at Ny-Ålesund can come from local emissions (EBC_{lo}) and long-range transport (EBC_{tr}).

$$EBC_{total} = EBC_{lo} + EBC_{tr} \quad (2)$$

Here, we assume that local emissions were generated by both random and continuous activities, which can be represented by high-frequency (IMF_1, $IMF_2 \ldots IMF_m$) and extremely low signals ($E_{low\text{-}lo}$), which were included in Trend. Hence, EBC_{lo} was defined as follows:

$$EBC_{lo} = IMF_1 + IMF_2 + \ldots + IMF_m + E_{low-lo} \quad (3)$$

Long-range transport is controlled by atmospheric circulation at various temporal scales (Stohl 2006); therefore, it can be expressed with specific frequency IMFs and as part of the signal in Trend. So EBC_{tr} were expressed as:

$$EBC_{tr} = IMF_{m+1} + IMF_{m+2} + IMF_{m+3} + \ldots + IMF_n + E_{low-tr}, \quad (4)$$

where $IMF_{m+1}, IMF_{m+2}, IMF_{m+3}, \ldots IMF_n$ are relatively low-frequency signals in IMFs and E_{low-tr} was the result from longer time scales of atmospheric circulation.

Based on these assumptions and principles of EEMD, the residual is understood to represent longer-term oscillation, which is associated with continuous local emissions and longer timescales of transport. That is:

$$Trend = E_{low-lo} + E_{low-tr} \quad (5)$$

In this study, EBC data were decomposed into 10 IMFs, corresponding to periods ranging from two hours to more than five days. Generally, the frequencies of local human activities are higher than those of long-range transport and they are characterized by diurnal variation or shorter periods of variations. Eleftheriadis et al. (2009) pointed out that diurnal variation in EBC concentration was less than ± 1 standard deviation range at Zeppelin Station during the summer months (JJA), suggesting that the diurnal variation was negligible; therefore, one day was chosen as a cut-off point and frequencies of one day or less were identified as being associated with local emissions, while variances lasting more than one day were ascribed to long-range transport. When Eqns. 1–5 were applied to the data measured at YRS, S2, S3 and S4, the results indicated that 60–80% of EBC at the YRS was from local emissions. The processes controlling BC in the atmospheric boundary layer include emissions, atmospheric transport and deposition or eventual ventilation (Wang et al. 2011). These are considered below.

Local emissions

EBC emission rates. The atmospheric dispersion factor (D, h m^{-3}) from the source to the receptor was calculated using the HYSPLIT model, and then the emission rates (Q, ng h^{-1}) were obtained by dividing the EBC concentrations (M, ng m^{-3}) from local emissions by the relevant dispersion factors, according to the equation: $Q = M/D$. EBC concentrations (M, ng m^{-3}) from local emissions were calculated using Eqn. 3. Here, a six-hour time average of the dispersion factor was set as the model output, and the average emission rate was calculated. A median value of 8.1 g h^{-1} was estimated, with a range from 1.0 to 25 g h^{-1}. The uncertainty in these factors was approximately a factor of two due to the uncertainty associated with measurements and accuracy of the dispersion model and meteorological data. According to the average PM 2.5 emission rates measured during on-road testing in South East Queensland, Australia, the emission factor was 15 g h^{-1} for diesel buses or 1.7 g h^{-1} for light-duty vehicles driving at an average speed of 50 km h^{-1} (Keogh et al. 2010). The emission rate at Ny-Ålesund was equivalent to about half the emission produced by a bus, or to emissions from about five light-duty vehicles constantly driving. Although emissions from local

human activities were miniscule compared to the emissions released from the mainland, these emissions in the vulnerable Arctic may change the physical and chemical properties of BC particles and more efficiently deposit to snow/ice surfaces (DeAngelo 2011).

EBC concentration distribution estimate. Using the HYSPLIT model, the spatial pattern of near-ground level EBC concentration due to local emissions was modelled every six hours and then averaged over the measurement period of this study. A contour plot of the average EBC concentration around Ny-Ålesund is shown in Fig. 4a. Hourly wind speed and direction at 2-m height during the measurement period is shown by the wind rose diagram (also in Fig. 4b). The prevailing winds during the experiments were typically either from the east–south-east or north–north-west. The concentration contour maps demonstrated that the trajectories of the EBC plumes released from Ny-Ålesund correlated well with the wind direction, and the plume shifted as wind changed in direction. The highest EBC concentration was about 14 ng m^{-3} at Ny-Ålesund, decreasing markedly with distance from the settlement as EBC was dispersed in the atmosphere. The concentrations of EBC reduced to 4.0 ng m^{-3} (30%) within 2 km of the source, with the majority of the downwind area having concentrations of less than 2.0 ng m^{-3}. However, the impact of these emissions was irregular, such that puffs were more likely to cover the southern sectors (south–south-east, south, and south–south-west), where the snow- or ice-covered surface was more sensitive to pollution compared to other exposed land, rather than the west–north-west sector.

EBC dry deposition estimate. In this study, dry deposition of EBC was estimated by the product of dry deposition velocities (V$_d$) and atmospheric EBC concentrations. Generally, V$_d$ was calculated by surface resistance, which was a function of aerodynamic resistance, friction velocity and surface type (Vignati et al. 2010). Here, a deposition velocity of 0.030 cm s^{-1} was chosen based on results presented by Nilsson & Rannik (2001) and Held et al. (2011) of eddy-covariance flux measurements in the Arctic, which was input to the model to determine the EBC dry deposition flux from local emissions around Ny-Ålesund. Each six-hour dry deposition flux was calculated; a contour map for the average of the whole period is shown in Fig. 5a. The deposition distribution pattern was similar to the concentration distributions, with the highest deposition of EBC directly downwind of the source, which was then immediately reduced to 4.0 ng m^{-2} h^{-1} (30% of the central value) within 2 km of the source. Major depositions occurred in glaciated areas in the south–south-west and south–south-east sector. EBC dry deposition from local emissions in summer ranged from 0.0 to 18 ng m^{-2} h^{-1} and total dry deposition (local emissions + long range transport) ranged from 4.3 to 32 ng m^{-2} h^{-1} (100–770 ng m^{-2} d^{-1}) within 10 km (Table 3). This is in the lower range of dry deposition flux over snow/ice (about 100–5300 ng m^{-2} day^{-1}) based on the observed BC depletion in the boundary layer in spring, including the period of biomass-burning that was documented (Spackman et al. 2010).

EBC wet deposition estimate. Wet deposition was also considered as a process controlling atmospheric BC concentration and affecting BC concentration in the
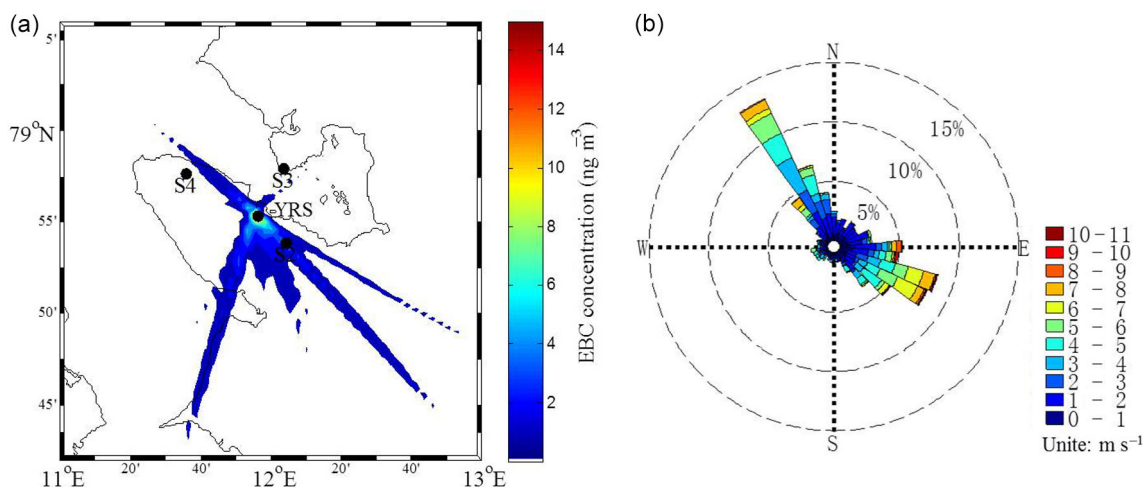
Fig. 4 (a) Contour plot of the average equivalent black carbon (EBC) concentrations during the entire experiment period at Yellow River Station (YRS) attributed to local emissions. (b) The wind rose plot was made for the entire experiment period at YRS. Individual wind direction measurements were accumulated and the relative frequency is shown as a percentage. Wind speed (m s^{-1}) is expressed by different colours.
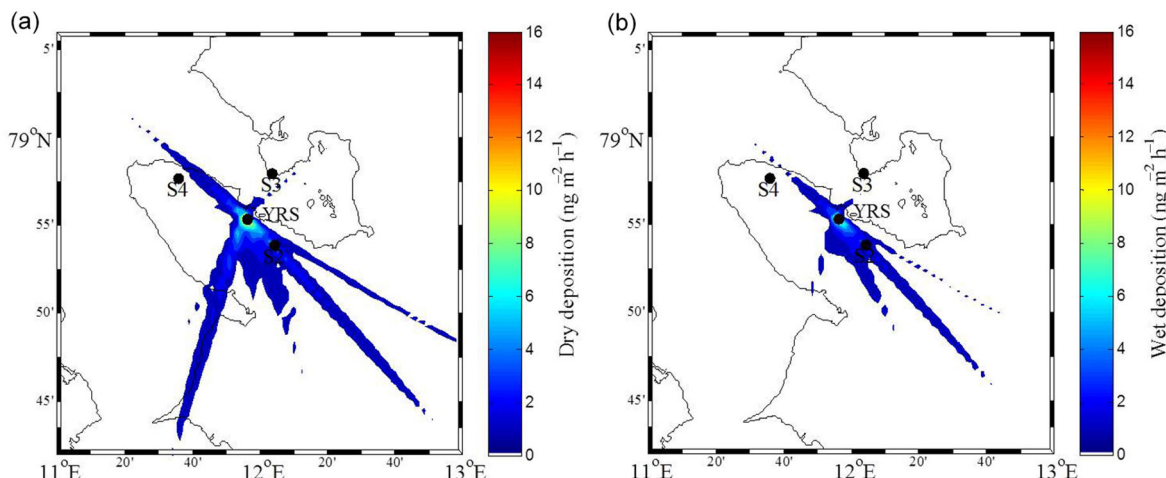
Fig. 5 (a) Contour plot of dry deposition averaged over the entire experiment period and (b) wet deposition from local emissions.

snow surface since the observation site was subjected to periods of heavy precipitation during summer, and a substantial fraction of aerosol might be washed out and deposited on the snow/ice surface (Liu et al. 2011). Here, wet deposition flux was calculated as follows:

$$F_w = C \times P = 10^{-3} \times EBC_{air} \times WR \times P, \quad (6)$$

where EBC_{air} is the EBC concentration in the air (ng m^{-3}), WR is the washout ratio, P is precipitation rate (mm h^{-1}) and F_w is the wet deposition flux (ng m^{-2} h^{-1}). The washout ratio,

$$WR = BC_{snow\ or\ rain}/BC_{air},$$

can be calculated by comparing of the amount of snow or rain with the concentration of BC in the air. Hegg et al. (2011) compared the washout ratio from fieldwork and the Scott washout ratio model (Scott 1978), and found that the washout ratio predicted by the model

was in reasonable agreement with the observed value. Hence, the Scott washout ratio was used in this study as follows:

$$WR(BC) = \frac{14000 \times M_S(0)}{BC_{air} \times P^{0.88}}$$
$$+ \frac{1000 \times F_{BC} \times (1 - 0.0441 \times P^{-0.88})}{1.56 + 0.44 \times IN\ P}, \quad (7)$$

where WR(BC) was the BC washout ratio, $M_s(0)$ was the concentration of BC (ng m^{-3}) in hydrometeors at the top of the riming zone, F_{BC} was scavenging efficiency, BC_{air} was the air concentration of BC, and P is the precipitation rate in mm h^{-1}. Here, we set $M_s(0) = 0.1$ BC_{air} (Scott's warm rain value) and $F_{BC} = 0.5$, since Hegg et al. (2011) reported that a predicted washout ratio using these two parameters agreed reasonably with the observed value for warm rain. The total precipitation was from the ECMWF database. The wet deposition due to

Table 3 Atmospheric deposition fluxes of equivalent black carbon in Ny-Ålesund, Svalbard, and Fairbanks, Alaska.

Station	Location	Time period	Sources	Estimated atmospheric black carbon flux (ng m^{-2} h^{-1})			Wet deposition (%)	References
				Dry deposition flux	Wet deposition flux	Total deposition flux		
Ny-Ålesund, Svalbard	11.60–12.06°E, 78.92–78.99°N 13–134 m a.s.l	July 2011	Local emissions	1.8–18	0.10–9.6	1.8–27	10–70	This work
			Total (local emissions + long-range transport)	4.3–32	2.1–12	6.4–44	22–44	
Fairbanks, Alaska	135–165°W, 65–75°N, 0.1–7.4 km a.s.l	April 2008	Total	4.2–220	–	–	91	Spackman et al. 2010

local emissions was calculated every six hours; the average was calculated for the whole period as shown in the contour map (Fig. 5b). Wet deposition from emissions ranged from 0.10 to 9.6 ng m^{-2} h^{-1}; total wet deposition ranged from 2.1 to 12 ng m^{-2} h^{-1} within 10 km (Table 3). Wet deposition accounted for 22–44% of total EBC deposition, which was lower than 78 ± 17% inferred from the AeroCom multimodel assessment (Textor et al. 2006) as well as the results from Spackman et al. (2010), who reported that wet deposition accounted for 91% of total BC deposition to the Arctic in spring and 85% in winter.

The total EBC depositions, which were defined as the sum of dry and wet deposition, were about 6.4–44 ng m^{-2} h^{-1}. Local emissions of BC contribute ca.15% to the total deposition within a radius of 10 km at Ny-Ålesund. This was similar to the figure reported for Svalbard by Norway's Climate and Pollution Agency: 20% of total deposition came from local emissions (Vestreng et al. 2009).

This analysis demonstrates that the environmental impacts of deposition from an individual source can be localized, with dispersion of pollutants in the atmosphere resulting in negligible environmental burdens beyond about 10 km downwind. Even though the pollution puffs from local emissions were more likely to pass over the glaciated areas in the southern sectors, the total deposition flux of EBC from local emission over these areas was less than 10 ng m^{-2} h^{-1}. If we assume that all of this BC is deposited on the top 1 cm of snow and the density of snow is 0.40 g cm^{-3}, then local emissions only contribute 1.8 ng BC per gram of snow each month. However, it is comparable to the average BC concentra-tion average (about 5 ng g^{-1}) in fresh snow previously measured in the same region in late May (Hegg et al. 2011). However, this analysis only considers a single emission source. A variety of uncertainties should be included in these calculations because the physical and chemical characteristics of BC are not constant. Rather, they involve different source and emission conditions, as well as the size, mixing state and chemical composition of BC particles. Hence, a far more sophisticated model should be used or developed to evaluate BC dispersion and deposition.

Long-range transport
Cluster analysis. Backward trajectories can provide information about the transport patterns and potential sources of the observed aerosols (Draxler & Hess 1998; Stohl 2006). The 10-day backward trajectories were calculated every six hours using HYSPLIT_4 and meteor-ological data to investigate the effect of long-range transport. Here, the arrival elevation of 540 m a.s.l was chosen for each trajectory calculation, which was the most representative arriving height (Worthy et al. 1994; Huang et al. 2010). Cluster analysis was used to classify the trajectories into different groups. The results of trajectories and cluster analysis (Fig. 6a) showed that Ny-Ålesund was impacted by three different atmospheric transport regimes during the study period. About 41% of air mass came from the Arctic Ocean, 31% originated from western Europe and 28% came from central Russia. Most of the air mass was confined to the north of 65°N, except the air mass from central Russia, which could originate from 60° N. This air mass could pass over settlement areas. The contribution of emissions from
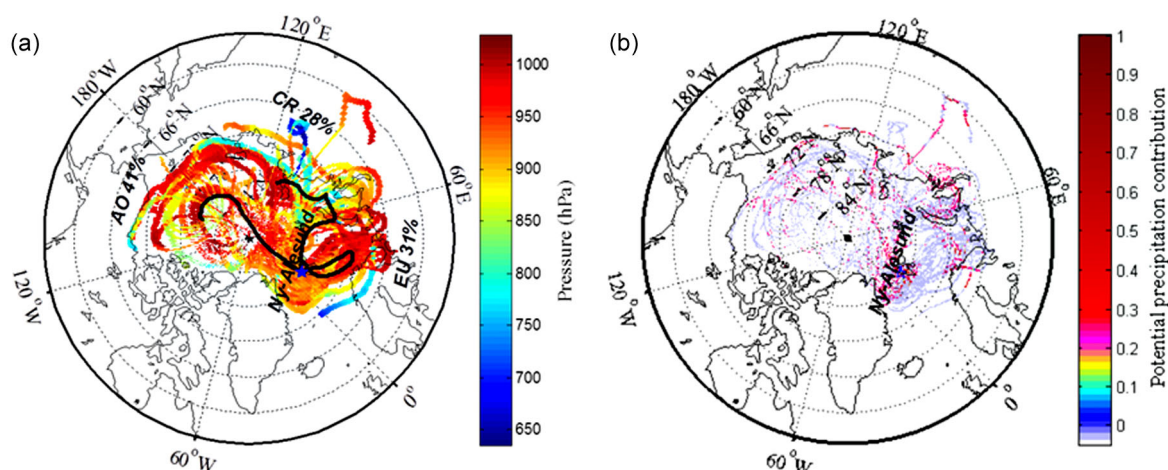
Fig. 6 (a) Ten-day back trajectories were coloured by air pressure and major transport pathways calculated by cluster analysis, labelled by identification of each cluster and frequency of occurrence. Both were generated by the HYSPLIT model. AO represents the Arctic Ocean sector, EU stands for western Europe and CR stands for central Russia. (b) Map of potential precipitation contribution function probability.

these areas to Arctic BC not only depends on sources but also the processes that occur en route, such as precipitation. Therefore the potential precipitation along each route and the temporal variance of each pattern were combined to interpret the contribution from each sector.

Potential precipitation contribution. Removal during transport is also an important factor affecting the efficiency of pollution transportation. The analysis of the potential precipitation contribution function (PPCF) was used to link atmospheric transport regimes with precipitation, given the possibility that rainfall occurred during the passage of the plume. The PPCF values for the grid cells $PPCF_{ij}$ were the conditional probabilities that an air parcel passing through the ij-th grid cell was accompanied with precipitation and was defined as:

$$\text{PPCF}_{ij} = \frac{mi_{ij}/N}{ni_{ij}/N} = \frac{P[B_{ij}]}{P[A_{ij}]}, \tag{8}$$

where n_{ij} was the total number of end points that fall in the ij-th cell, and m_{ij} was the number of end points in the same cell that were associated with precipitation. $P(B_{ij})$ was the probability of precipitation in the ij-th cell, and $P(A_{ij})$ was the probability of trajectories that pass over the ij-th cell. To reduce the effect of small values of n_{ij}, an arbitrary weight function $W(n_{ij})$ was applied to downweight the $PPCF_{ij}$ values. Here, the weight function $W(n_{ij})$, given by Hopke et al. (1995), was defined as:

$$W(n_{ij}) \begin{cases} 1.0 \; if \; n_{ij} \geq 4 \\ 0.75 \; if \; n_{ij} = 3 \\ 0.50 \; if \; n_{ij} = 2 \\ 0.25 \; if \; n_{ij} = 1 \end{cases} \tag{9}$$

Combining the heights of transport pathway and PPCF distribution shown in Fig. 6, indicated that air masses from western Europe experience less precipitation than air masses passing over central Russia. Western Europe was therefore a probable source for the BC ending up in Svalbard, since pollutants from central Russia were more likely to be washed out en route to the Arctic archipelago. Because of the precipitation, only pollutions originating in central Russia that existed at a higher atmospheric level were likely to be transported to the Arctic through free troposphere-level transport. However, there was no correlation with air mass back-trajectories and EBC concentrations, suggesting that the contribution of long-range transport might be not significant, while local emissions might be responsible for the elevated EBC observed at the Ny-Ålesund community.

Conclusions

Higher concentrations of EBC were observed within Ny-Ålesund compared with measurements outside the settlement and these were attributed to local emissions. It is estimated that about 60–70% of EBC in Ny-Ålesund was associated with local emissions, whereas emissions from outside the Arctic had less impact on local BC concentrations as a result of precipitation scavenging (Stohl 2006). Additionally, meteorological parameters appear to be of minor importance and could only explain 19% the observed EBC variability.

The average emission rate at Ny-Ålesund was 8.1 g h^{-1}, equivalent to the BC emissions from about five light duty vehicles, or half the BC emissions from a bus, in constant operation. Our modelling results indicate that BC dry deposition from local emissions at Ny-Ålesund was 0.0–1.8 ng m^{-2} h^{-1}, and wet deposition was 0.0 to 9.6 ng m^{-2} h^{-1} within 10 km. Dispersion and deposition patterns at Ny-Ålesund suggested that local emissions decreased to 20% within 10 km and plumes tended to affect the area to the south of the settlement.

Overall, the limited data from this study suggested that local emissions made a major contribution to EBC concentrations at Ny-Ålesund within 10 km. Even though Zeppelin Station is located 474 m a.s.l, it is still influenced by ship emissions during summer (Eckhardt et al. 2013). Researchers aiming to study pristine environments in the Arctic should consider the effects of these local emissions on air quality.

References

Barrie L.A. 1996. Occurrence and trends of pollution in the Arctic troposphere. In E. Wolff & R.C. Bales (eds.): *Chemical exchange between the atmosphere and polar snow.* Pp. 93–130. New York: Springer.

Bourgeois Q. & Bey I. 2011. Pollution transport efficiency toward the Arctic: sensitivity to aerosol scavenging and source regions. *Journal of Geophysical Research—Atmospheres 116*, D08213, doi: 10.1029/2010JD015096.

Corbett J.J., Lack D.A., Winebrake J.J., Harder S., Silberman J.A. & Gold M. 2010. Arctic shipping emissions inventories and future scenarios. *Atmospheric Chemistry and Physics 10*, 9689–9704.

Dalsøren S.B., Endresen Ø., Isaksen I.S.A., Gravir G. & Sørgård E. 2007. Environmental impacts of the expected increase in sea transportation, with a particular focus on oil and gas scenarios for Norway and northwest Russia. *Journal of Geophysical Research—Atmospheres 112*, D02310, doi: 10.1029/2005JD006927.

DeAngelo B.E. 2011. *An assessment of emissions and mitigation options for black carbon for the Arctic Council. Technical report of the Arctic Council Task Force on Short-Lived Climate Forcers.* Tromsø: Arctic Council.

Devasthale A., Willén U., Karlsson K.-G. & Jones C.G. 2010. Quantifying the clear-sky temperature inversion frequency and strength over the Arctic Ocean during summer and winter seasons from AIRS profiles. *Atmospheric Chemistry and Physics 10*, 5565–5572.

Di Liberto L., Angelini F., Pietroni I., Cairo F., Di Donfrancesco G., Viola A., Argentini S., Fierli F., Gobbi G., Maturilli M., Neuber R. & Snels1 M. 2012. Estimate of the Arctic convective boundary layer height from Lidar observations: a case study. *Advances in Meteorology 2012*, 851927, doi: 10.1155/2012/851927.

Doherty S.J., Warren S.G., Grenfell T.C., Clarke A.D. & Brandt R.E. 2010. Light-absorbing impurities in Arctic snow. *Atmospheric Chemistry and Physics 10*, 11647–11680.

Draxler R.R. & Hess G.D. 1998. An overview of the HYSPLIT_4 modelling system for trajectories, dispersion, and deposition. *Australian Meteorological Magazine 47*, 295–308.

Eckhardt S., Hermansen O., Grythe H., Fiebig M., Stebel K., Cassiani M., Baecklund A. & Stohl A. 2013. The influence of cruise ship emissions on air pollution in Svalbard—a harbinger of a more polluted Arctic? *Atmospheric Chemistry and Physics 13*, 8401–8409.

Eleftheriadis K., Vratolis S. & Nyeki S. 2009. Aerosol black carbon in the European Arctic: measurements at Zeppelin Station, Ny-Ålesund, Svalbard from 1998–2007. *Geophysical Research Letters 36*, L02809, doi: 10.1029/2008GL035741.

Flanner M.G., Zender C.S., Hess P.G., Mahowald N.M., Painter T.H., Ramanathan V. & Rasch P.J. 2009. Springtime warming and reduced snow cover from carbonaceous particles. *Atmospheric Chemistry and Physics 9*, 2481–2497.

Granier C., Niemeier U., Jungclaus J.H., Emmons L., Hess P., Lamarque J.F., Walters S., & Brasseur G.P. 2006. Ozone pollution from future ship traffic in the Arctic northern passages. *Geophysical Research Letters 33*, L13807, doi: 10.1029/2006GL026180.

Hadley O.L. & Kirchstetter T.W. 2012. Black-carbon reduction of snow albedo. *Nature Climate Change 2*, 437–440.

Hansen A.D.A., Turner J.R. & Allen G.A. 2007. An algorithm to compensate Aethalometer™ data for the effects of optical shadowing and scattering. Paper presented at the 5th Asian Aerosol Conference. 26–29 August, Kaohsiung, Taiwan.

Hegg D.A., Clarke A.D., Doherty S.J. & Ström J. 2011. Measurements of black carbon aerosol washout ratio on Svalbard. *Tellus Series B 63*, 891–900.

Heintzenberg J. & Leck C. 1994. Seasonal variation of the atmospheric aerosol near the top of the marine boundary layer over Spitsbergen related to the Arctic sulphur cycle. *Tellus Series B 46*, 52–67.

Held A., Orsini D.A., Vaattovaara P., Tjernström M. & Leck C. 2011. Near-surface profiles of aerosol number concentration and temperature over the Arctic Ocean. *Atmospheric Measurement Techniques 4*, 1603–1616.

Hermansen O., Wasseng J., Bäcklund A., Noon B., Hennig T., Schulze D. & Barth V.L. 2011. *Air quality Ny-Ålesund. Monitoring of local air quality 2008–2010. Measurement results.* Kjeller, Norway: Norwegian Institute for Air Research.

Hirdman D., Burkhart J.F., Sodemann H., Eckhardt S., Jefferson A., Quinn P.K., Sharma S., Ström J. & Stohl A. 2010. Long-term trends of black carbon and sulphate aerosol in the Arctic: changes in atmospheric transport and source region emissions. *Atmospheric Chemistry and Physics 10*, 9351–9368.

Hirdman D., Sodemann H., Eckhardt S., Burkhart J.F., Jefferson A., Mefford T., Quinn P.K., Sharma S., Ström J. & Stohl A. 2010. Source identification of short-lived air pollutants in the Arctic using statistical analysis of measurement data and particle dispersion model output. *Atmospheric Chemistry and Physics 10*, 669–693.

Hopke P.K., Barrie L.A., Li S.M., Cheng M.D., Li C. & Xie Y. 1995. Possible sources and preferred pathways for biogenic and non-sea-salt sulfur for the High Arctic. *Journal of Geophysical Research—Atmospheres 100*, 16595–16603.

Huang L., Gong S.L., Sharma S., Lavoué D. & Jia C.Q. 2010. A trajectory analysis of atmospheric transport of black carbon aerosols to Canadian High Arctic in winter and spring (1990–2005). *Atmospheric Chemistry and Physics 10*, 5065–5073.

Jacob D.J., Crawford J.H., Maring H., Clarke A.D., Dibb J.E., Emmons L.K., Ferrare R.A., Hostetler C.A., Russell P.B., Singh H.B., Thompson A.M., Shaw G.E., McCauley E., Pederson J.R. & Fisher J.A. 2010. The Arctic Research of the Composition of the Troposphere from Aircraft and Satellites (ARCTAS) mission: design, execution, and first results. *Atmospheric Chemistry and Physics 10*, 5191–5212.

Johnson M.R., Devillers R.W. & Thomson K.A. 2011. Quantitative field measurement of soot emission from a large gas flare using Sky-LOSA. *Environmental Science & Technology 45*, 345–350.

Keogh D.U., Kelly J., Mengersen K., Jayaratne R., Ferreira L. & Morawska L. 2010. Derivation of motor vehicle tailpipe

particle emission factors suitable for modelling urban fleet emissions and air quality assessments. *Environmental Science and Pollution Research 17*, 724–739.

Klonecki A., Hess P., Emmons L., Smith L., Orlando J. & Blake D. 2003. Seasonal changes in the transport of pollutants into the Arctic troposphere-model study. *Journal of Geophysical Research—Atmospheres 108*, 8367, doi: 10.1029/2002JD002199.

Koch D., Bauer S.E., Del Genio A., Faluvegi G., McConnell J.R., Menon S., Miller R.L., Rind D., Ruedy R., Schmidt G.A. & Shindell D. 2011. Coupled aerosol-chemistry–climate twentieth-century transient model investigation: trends in short-lived species and climate responses. *Journal of Climate 24*, 2693–2714.

Lack D., Lerner B., Granier C., Baynard T., Lovejoy E., Massoli P., Ravishankara A.R. & Williams E. 2008. Light absorbing carbon emissions from commercial shipping. *Geophysical Research Letters 35*, L13815, doi: 10.1029/2008GL033906.

Law K.S. & Stohl A. 2007. Arctic air pollution: origins and impacts. *Science 315*, 1537–1540.

Lee D.S., Pitari G., Grewe V., Gierens K., Penner J.E., Petzold A., Prather M.J., Schumann U., Bais A., Berntsen T., Iachetti D., Lim L.L. & Sausen R. 2010. Transport impacts on atmosphere and climate: aviation. *Atmospheric Environment 44*, 4678–4734.

Liu J.F., Fan S.M., Horowitz L.W. & Levy H. 2011. Evaluation of factors controlling long-range transport of black carbon to the Arctic. *Journal of Geophysical Research—Atmospheres 116*, D04307, doi: 10.1029/2010JD015145.

Nilsson E.D. & Rannik Ü. 2001. Turbulent aerosol fluxes over the Arctic Ocean 1. Dry deposition over sea and pack ice. *Journal of Geophysical Research—Atmospheres 106*, 32125–32137.

Nyeki S., Bauer H., Puxbaum H., Dye C., Teinila K., Hillamo R., Ström J. & Eleftheriadis K. 2005. Comparison of black carbon concentrations derived by filter-based light transmission and thermo-optical techniques for Arctic aerosol. Paper presented at European Aerosol Conference 2005. 28 August–2 September, Ghent, Belgium.

Quinn P.K., Stohl A., Arneth A., Berntsen T., Burkhart J.F., Christensen J., Flanner M., Kupiainen K., Lihavainen H., Shepherd M., Shevchenko V., Skov H. & Vestreng V. 2011. *The impact of black carbon on Arctic climate*. Oslo: Arctic Monitoring and Assessment Programme.

Scott B.C. 1978. Parameterization of sulfate removal by precipitation. *Journal of Applied Meteorology 17*, 1375–1389.

Sharma S., Andrews E., Barrie L.A., Ogren J.A. & Lavoué D. 2006. Variations and sources of the equivalent black carbon in the High Arctic revealed by long-term observations at Alert and Barrow: 1989–2003. *Journal of Geophysical Research—Atmospheres 111*, D14208, doi: 10.1029/2005JD006581.

Sharma S., Lavoué D., Cachier H., Barrie L.A. & Gong S.L. 2004. Long-term trends of the black carbon concentrations in the Canadian Arctic. *Journal of Geophysical Research—Atmospheres 109*, D15203, doi: 10.1029/2003JD004331.

Shindell D. & Faluvegi G. 2009. Climate response to regional radiative forcing during the twentieth century. *Nature Geoscience 2*, 294–300.

Solomon S., Qin D., Manning M., Chen Z., Marquis M., Averyt K.B., Tignor M. & Miller H.L. Jr. (eds.) 2007. *Climate change 2007. The physical science basis: contribution of Working Group I to the fourth assessment report of the Intergovernmental Panel on Climate Change*. Cambridge: Cambridge University Press.

Spackman J.R., Gao R.S., Neff W.D., Schwarz J.P., Watts L.A., Fahey D.W., Holloway J.S., Ryerson T.B., Peischl J. & Brock C.A. 2010. Aircraft observations of enhancement and depletion of black carbon mass in the springtime Arctic. *Atmospheric Chemistry and Physics 10*, 9667–9680.

Stohl A. 2006. Characteristics of atmospheric transport into the Arctic troposphere. *Journal of Geophysical Research—Atmospheres 111*, D11306, doi: 10.1029/2005JD006888.

Textor C., Schulz M., Guibert S., Kinne S., Balkanski Y., Bauer S., Berntsen T., Berglen T., Boucher O., Chin M., Dentener F., Diehl T., Easter R., Feichter H., Fillmore D., Ghan S., Ginoux P., Gong S., Grini A., Hendricks J., Horowitz L., Huang P., Isaksen I., Iversen I., Kloster S., Koch D., Kirkevåg A., Kritjansson J.E., Krol M., Lauer A., Lamarque J.F., Liu X., Montanaro V., Myhre G., Penner J., Pitari G., Reddy S., Seland Ø., Stier P., Takemura T. & Tie X. 2006. Analysis and quantification of the diversities of aerosol life cycles within AeroCom. *Atmospheric Chemistry and Physics 6*, 1777–1813.

Tjernström M. 2005. The summer Arctic boundary layer during the Arctic Ocean Experiment 2001 (AOE-2001). *Boundary-Layer Meteorology 117*, 5–36.

Tjernström M. & Graversen R.G. 2009. The vertical structure of the lower Arctic troposphere analysed from observations and the ERA-40 reanalysis. *Quarterly Journal of the Royal Meteorological Society 135*, 431–443.

Vestreng V., Kallenborn R. & Økstad E. 2009. *Norwegian Arctic climate: climate influencing emissions, scenarios and mitigation options at Svalbard*. Oslo: Climate and Pollution Agency.

Vignati E., Karl M., Krol M., Wilson J., Stier P. & Cavalli F. 2010. Sources of uncertainties in modelling black carbon at the global scale. *Atmospheric Chemistry and Physics 10*, 2595–2611.

Wang Q., Jacobs D.J., Fisher J.A., Mao J., Leibensperger E.M., Carouge C.C., Le Sager P., Kondo Y., Jimenez J.L., Cubison M.J. & Doherty S.J. 2011. Sources of carbonaceous aerosols and deposited black carbon in the Arctic in winter–spring: implications for radiative forcing. *Atmospheric Chemistry and Physics 11*, 12453–12473.

Worthy D.E.J., Trivett N.B.A., Hopper J.F., Bottenheim J.W. & Levin I. 1994. Analysis of long-range transport events at Alert, Northwest Territories, during the Polar Sunrise Experiment. *Journal of Geophysical Research 99*, 25329–25344.

Wu Z. & Huang N.E. 2004. A study of the characteristics of white noise using the empirical mode decomposition method. *Proceedings of the Royal Society A: Mathematical, Physical & Engineering Sciences 460*, 1597–1611.

Wu Z.H. & Huang N.E. 2009. Ensemble empirical mode decomposition: a noise assisted data analysis method. *Advances in Adaptive Data Analysis 1*, doi: 10.1142/S1793536909000047.